

Grafted Polythiophene Pendent Polymer Brushes and their Electronanopatterning

Edward L. Foster^a, Al Christopher C. de Leon^a, Peng-Fei Cao^b, Eugene B. Caldon^{b,c}, and Rigoberto C. Advincula^{a,b,c*}

^aDepartment of Macromolecular Science and Engineering, Case Western Reserve University, Cleveland, OH 44106, USA

^bCenter for Nanophase Materials Sciences and Chemical Sciences Division, Oak Ridge National Laboratory, Oak Ridge, TN 37830, USA

^cDepartment of Chemical and Biomolecular Engineering and Institute for Advanced Materials and Manufacturing, University of Tennessee, Knoxville, TN 37996, USA

*Correspondence to: R. C. Advincula (E-mail: rca41@case.edu)

Abstract

Electrochemical nanolithography using grafted polymer brushes with terthiophene (3T) pendent was investigated. The film was fabricated by surface electropolymerization of a reversible addition–fragmentation chain-transfer agent macroinitiator containing a 3T pendant molecule and the subsequent polymer brush growth from a 3T functionalized methacrylate monomer (3T-Methacrylate). Electrochemical nanolithography and patterning were done using conducting atomic force microscopy (C-AFM) enabling precise nanopattern fabrication. In contrast to direct nanowriting, dip pen nanolithography, and nanolithographic additive manufacturing, the electrochemical nanolithography can be readily facilitated by applying a bias voltage between a conductive AFM tip and the grafted polymer brush film at ambient conditions and without ink transfer. The height and electrical resistance of the nanopatterns were dependent on the writing parameters (i.e. applied bias voltage and scan rate).

Keywords: Nanolithography; Atomic Force Microscopy; Conducting polymer; Polythiophene; Electropolymerization

1. Introduction

Micro- and nanolithography are used to fabricate patterns with sizes ranging from the milli- to nanometer scale. The optimization of these properties has contributed to the manufacturing of integrated circuits (ICs), microchips, optoelectronics, and molecular electronic devices [1–5]. Conventional lithography techniques either require the use of a template/mask or other mask free methods. Masked lithography uses masks to transfer patterns to substrates, which include photolithography, soft lithography, and nano-imprint lithography [6,7]. The advantage of these techniques includes capability to pattern large areas and high-throughput fabrication for commercial applications.

Alternatively, mask free lithography techniques fabricate arbitrary patterns by serial writing without the use of masks. These techniques include electron beam and focused ion beam lithography [8]. These methods are advantageous because they can create patterns in a serial manner, allowing for ultrahigh-resolution patterning. However, the current throughput of mask free techniques is limited by their slow writing capabilities, making them, to date, relatively unrealistic for mass production [6]. In addition, electron beam lithography is highly specialized and equipment-intensive, making it expensive and less accessible to researchers [9].

An alternative mask free technique, scanning probe microscopy (SPM), has become a popular method of preparing nanoscale structures [10] due to its relatively low cost and high resolution, thereby, making it an adoptable technique by both academic and industrial researchers for applications including bio-electronics, bio-sensors, gas sensors, and rapid and relatively inexpensive prototype fabrication technique for research and development purposes [9,10]. Bias assisted lithography is an SPM technique, similar to current sensing atomic force microscopy (CS-AFM) and conducting AFM (C-AFM), which uses a voltage bias AFM tip capable of inducing electrochemical polymerization or oxidation of an electroactive film on a conducting substrate to achieve controlled and well-defined nanostructures [11]. Control over the spatial and electrical properties of the resulting nanostructures can be achieved by varying the applied bias and writing speed [12].

To date, several methods have been used to functionalize conducting surfaces with electroactive organic materials and films (i.e. spin coating, Langmuir-Blodgett, or layer-by-layer (LBL) techniques) [12–18]. However, these techniques suffer drawbacks such as lack of film thickness control, film stability, and low grafting density. An alternative way to functionalize surfaces is by performing surface-initiated polymerization (SIP) from surface-bound initiators forming polymer brushes [19–24]. SIP allows monomers of interest to be controllably grown from the surface-bound initiators. Therefore, the properties of polymer brush films generated by SIP can be modified by varying parameters related to the type of initiation mechanism, grafting density, and degree of polymerization [19]. This provides a uniform surface coverage of the initiating functional groups with the possibility for obtaining block copolymers or mixed polymer brush systems. SIP using controlled living free radical polymerization techniques, such as reversible-addition fragmentation chain transfer (RAFT), atom transfer radical polymerization, and nitroxide mediated polymerization, permits the synthesis of tethered polymers with various functionalities, and control over molecular weight, polydispersity, and macromolecular architectures [19]. Among the controlled living radical polymerization techniques, RAFT polymerization possesses a unique advantage due to its relative simplicity and functional group tolerance [25]. Another advantage of RAFT polymerization includes conventional free radical polymerization being readily convertible into a RAFT process by adding an appropriate RAFT agent, such as a dithioester, dithiocarbamate, or trithiocarbonate

compound, while other parameters including monomer, initiator, solvent, and temperature, can be kept constant [25,26].

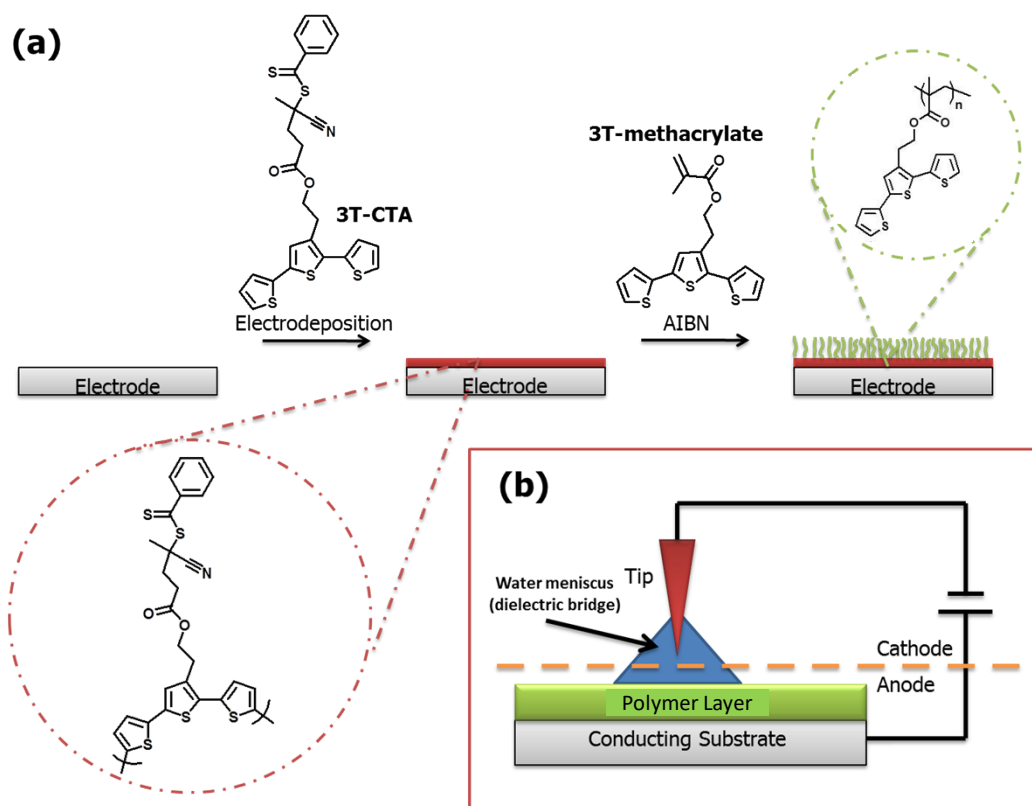


Figure 1. Illustration of (a) polymer brush film fabrication and (b) electrochemical nanolithography using current sensing AFM (note: the yellow line indicates the separation between the cathodic and anodic regions)

Herein the fabrication of precisely controlled nanopatterns on precursor polymer (polythiophene) brushes using the electrochemical nanolithography technique is reported (Figure 1). Unlike direct nanowriting on an insulating solid-state film in an electrolyte solution, the patterning feature can be readily done by applying a bias voltage between a conductive AFM tip and the polymer brush film at ambient conditions in air. The resulting localized patterns can be characterized by investigating the surface morphology (AFM topographic change) and electrical properties of the conductive pattern (current mapping). These patterns rely on various parameters such as applied bias voltage and scan rate.

2. Materials and methods

2.1. Materials

Reagent chemicals tetrabutylammonium hexafluorophosphate (TBAH, 99%), CuBr (99%), triethylamine (99%), bromine (99%), and 2-(tributylstannyl)thiophene were all purchased from Sigma-Aldrich, and were used without further purification, unless otherwise indicated. Trans-

dichlorobis(triphenylphosphine)palladium, ethylthiophene-3-acetate (98%), and terthiophene (99%) were all purchased from Alfa Aesar, and were used without further purification. Deionized water, methanol (MeOH), dimethylformamide (DMF), isopropanol, n-hexane, acetonitrile (ACN), and tetrahydrofuran (THF) were used in cleaning the substrates (i.e. indium tin oxide (ITO) and gold slides), synthesis, and polymerization reactions. Terthiophene (3T)-chain transfer agent (CTA) and 3T-methacrylate were synthesized according to previous literature [27].

2.2. Surface preparation

The substrates were cut into 2.5×0.7 cm slides. The ITO slides were then cleaned using an Alconix solution, followed by sonicating separately in isopropanol, hexane, and toluene for 10 min each. The ITO slides were then dried under N_2 gas, followed by plasma cleaning for 3 min. The gold slides were rinsed with ethanol, dried under N_2 gas, and plasma cleaned for 30 s. The slides were either used immediately or stored in a desiccator.

2.3. Electropolymerization

The electropolymerization of 3T-CTA was performed via cyclic voltammetry (CV) using an Autolab PGSTAT 12 Potentiostat (Metrohm) in a standard three-electrode measuring cell (a fabricated electrochemical cell with a diameter of 1.0 cm and volume of 0.785 cm^3 , made of Teflon) with Pt wire as the counter, Ag/AgCl wire as the reference, and the ITO substrate as the working electrode. All electrodepositions were performed using CV in ACN at a potential of 0-1.2 V and scan rate of 50 mV/s for 10 cycles. After the electrodeposition, the resulting film was washed with ACN twice.

2.4. Surface initiated RAFT polymerization

In a typical reaction, SI-RAFT polymerization of 3T-methacrylate was performed as such. 1.0 g (2.8 mmol) of 3T-methacrylate and 0.77 mg (4.7×10^{-3} mmol) of 2,2-azobis(isobutyronitrile) (AIBN) as the supporting electrolyte were dissolved in 8 mL of dry toluene and magnetically stirred in a N_2 atmosphere for 30 min. Afterwards, 3 freeze-pump-thaw cycles were performed on the mixture. The solution was transferred to another Schlenk tube containing the coated gold or ITO substrate. Polymerization was performed for 72 h at 80 °C. The slide was removed and carefully washed by toluene and THF, and subsequently dried with N_2 and further in a vacuum desiccator prior to any measurements.

2.5. Characterization

All nanolithographic electrochemical patterning has been done with a commercial CS-AFM (Agilent 5500 atomic force microscopy). A bias voltage between a conductive substrate and a tip was applied using the conductive tip (Pt-Ir coated tips with 20 nm radius; Agilent). The free frequency was 10–17 kHz, while the spring constant was 0.07–0.4 $N \text{ m}^{-1}$. The patterning process was conducted by applying substrate-to-tip bias voltage under ambient conditions. The particular patterns can be driven by using the Picolith (Agilent) software. All AFM topographic images were filtered and analyzed using Scanning Probe Image Processor (SPIP, Imagemet.com) or Gwyddion 2.19 software. CV was performed in a conventional three-electrode cell, using an Autolab PGSTAT 12 Potentiostat (Metrohm USA). The potentiostat was controlled

using GPES software (version 4.9). Fourier transform infrared (FTIR) spectroscopy was performed on a Digilab FTS 7000 FTIR spectrometer between 2000 and 600 cm^{-1} using a resolution of 8 cm^{-1} .

3. Results and discussion

Electropolymerization of heteroaromatic monomers to form π -conjugated conducting polymers has been investigated heavily [28,29]. Polythiophenes, in particular, are one of the most well-studied polymeric systems [30–32]. The electropolymerization mechanism goes through a radical cation coupling, which can be accessed through potentiodynamic or potentiostatic methods [33,34]. Our group has reported the electrodeposition of high optical quality ultrathin films of conjugated polymer networks on conducting substrates via electrochemical methods [27,32,35]. Electrodeposition of a conducting polymer macroinitiator on a planar electrode substrate is a plausible route [27]. The use of the electropolymerization method in immobilizing initiators or CTA on surfaces also enjoys the advantage of employing only one type of electroactive initiator or CTA to any conducting substrates. This approach avoids the synthesis of different types of surface-coupling agents [27].

The electrodeposition and the subsequent electrochemical nanolithography are illustrated in Figure 1. The electropolymerization of the macroinitiator was performed in a three-electrode cell, with an ACN solution containing terthiophene with CTA derivative (3T-CTA, 0.5 mM) and 0.1 M TBAH. This was done using cyclic voltammetry (CV) at a scan rate of 50 mV/s and by sweeping the potential from 0 to 1.2 V versus the Ag/AgCl reference electrode and Pt counter electrode on non-transparent gold (Au) or transparent ITO substrates. Note that the reason for using two different types of substrates was so that different characterization techniques could be used to characterize the film. The CV diagram is depicted in Figure 2. The CV diagram of the electrodeposition process shows a reversible redox process due to the oxidation (anodic) and reduction (cathodic) scans. As shown in Figure 2, the onset potential of the first cycle in the anodic peak is around 0.70 V. This anodic peak is due to the oxidation of polymeric terthiophene. The oxidation onset becomes lower (i.e. 0.45 V) in the second cycle onward [36,37]. This behavior is typical for most electrodeposition procedures involving CV. Here, the more conjugated polymer species formed resulted in a lower oxidation potential onset for doping. The corresponding reduction peak was observed at around 0.63 V due to the dedoping of the polythiophene [38]. The substrates were then rinsed with ACN, THF, back with ACN, and finally dried under vacuum.

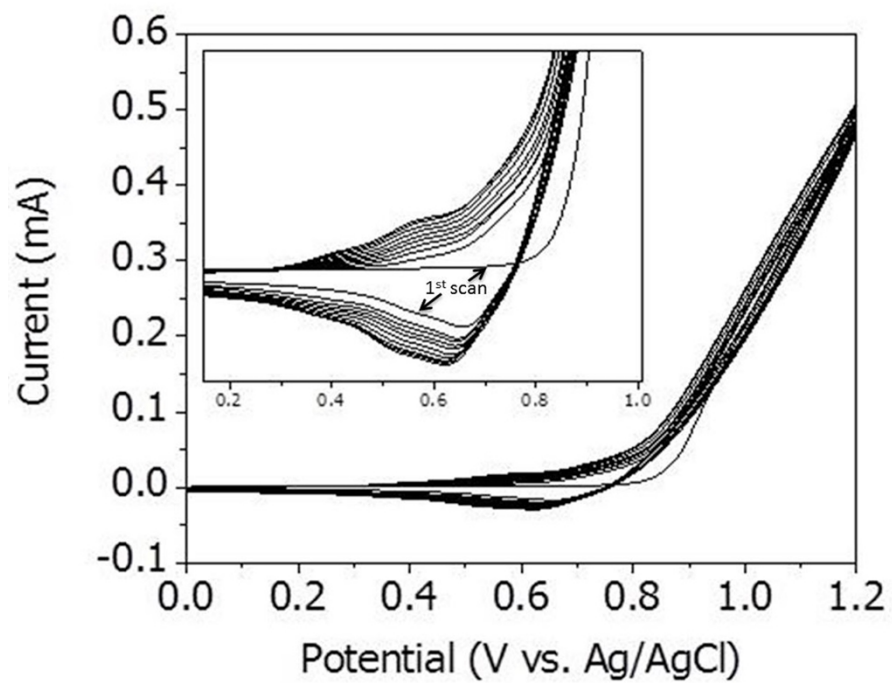


Figure 2. Cyclic voltammogram of electrodeposition of 3T-CTA. Inset is the magnified cyclic voltammogram from 0.2 V to 1.0 V.

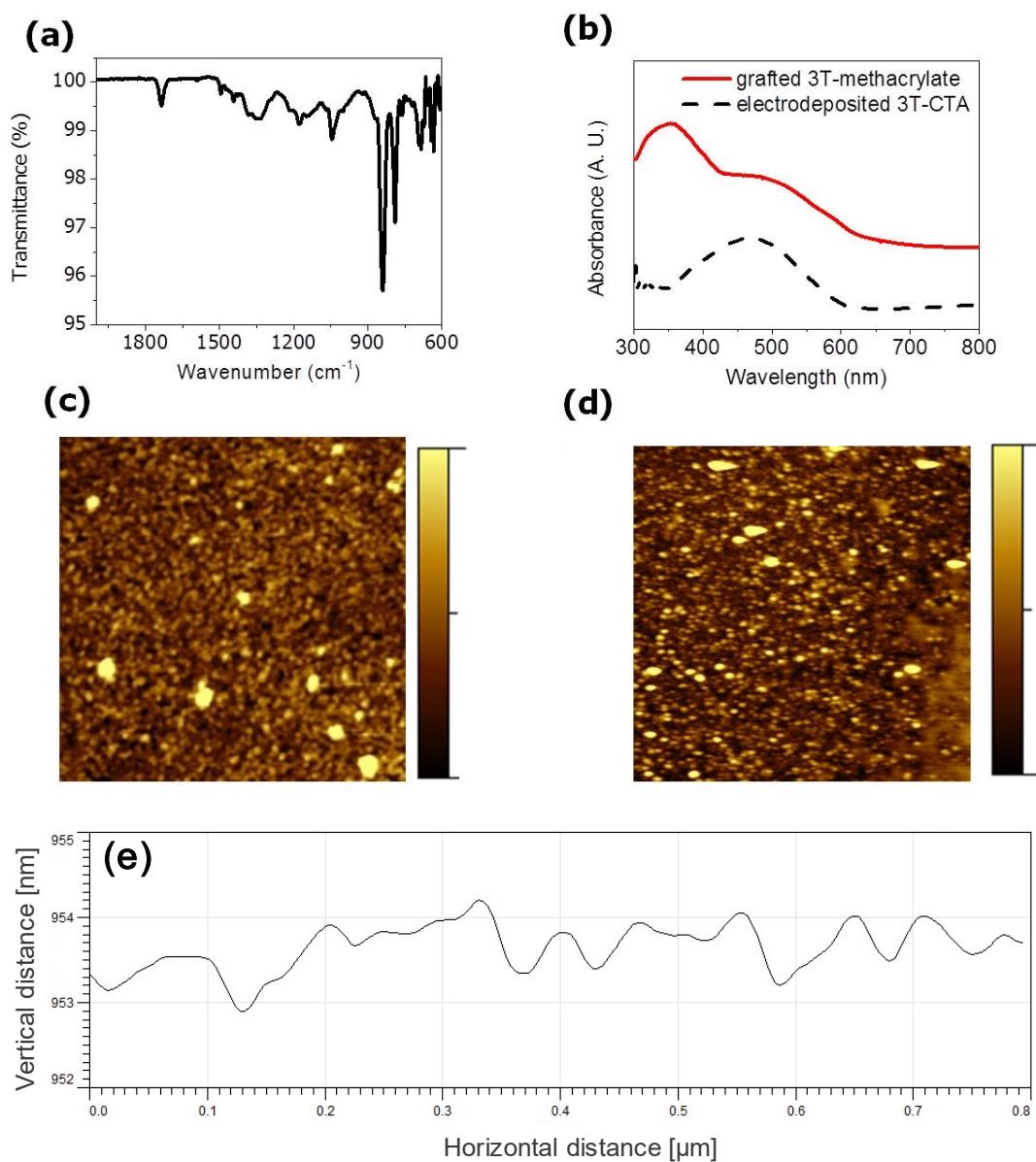


Figure 3. (a) FT-IR spectra of electrodeposited 3T-CTA. (b) UV-vis spectra of electrodeposited 3T-CTA and grafted 3T-methacrylate. $2 \times 2 \mu\text{m}$ AFM topography (z range 10 nm) images of (c) electrodeposited 3T-CTA and (d) grafted 3T-methacrylate. (e) Line profile of 3T-polymer brush.

The successful surface modification with the conjugate polymer network of 3T-CTA was confirmed by ellipsometry and Fourier-transform infrared (FTIR) spectroscopy. The electrodeposited film at 10 cycles gave an average thickness of 6.23 ± 0.78 nm. The FTIR spectrum (Figure 3a) reveals the distinct peaks of both the conjugated polymer network (CPN) composed of terthiophene repeating units and the RAFT CTA moiety. For example, a strong characteristic out of plane broad vibrational peak at 839 cm^{-1} arising from

C-H ring of the thiophene rings is clearly seen [37,39]. Similarly, the peak at 1735 cm^{-1} is attributed to the carbonyl functional group on the CTA moiety [39].

Surface-initiated polymerization (SIP) of 3T-methacrylate was performed by placing 1.0 g of it (chemical structure shown in Figure 1a) and 0.77 mg of AIBN initiator in 8 mL of dry toluene. AIBN was chosen as the initiator as it partially decomposes into a relatively stable radical and helps control the molecular weight increase from the surface and maintains the presence of active living end groups [27]. Three freeze pump thaw cycles were performed on the solution mixture. Afterwards, the solution was then transferred via syringe to a degassed Schlenk tube containing the 3T-CTA film on either Au or ITO coated substrate. The polymerization was then allowed to proceed for 72 h. It is important to mention that the use of the methacrylate group was chosen because of its good polymerizability using RAFT polymerization. Additional types of monomers could also be used (i.e. styrene and acrylates) [19].

After polymerization, the brush thickness was found to be $24.8 \pm 2.2\text{ nm}$ using ellipsometry. Similarly, UV-vis spectroscopy was also employed to monitor the progress of the surface modification (Figure 3b). The absorption spectra are characterized by a broad peak at 465 nm, attributed to the π to π^* transition of the polythiophene peak, which confirms the presence of the CPN from the electrodeposited 3T-CTA [40]. After the SI-RAFT polymerization of 3T-methacrylate occurred, a peak was observed at 355 nm, indicating the successful growth of the polymer brush. AFM topographic image analysis also supported the surface modification as shown by the differences in topography after each step (Figure 3c and 3d). Bigger globular domains were formed after the formation of the 3T-methacrylate brush (Figure 3d) as compared to the electrodeposited 3T-CTA (Figure 3c). In addition, it should be mentioned that the film growth globules. The height of these globules is $\sim 0.5\text{ nm}$ (Figure 3e).

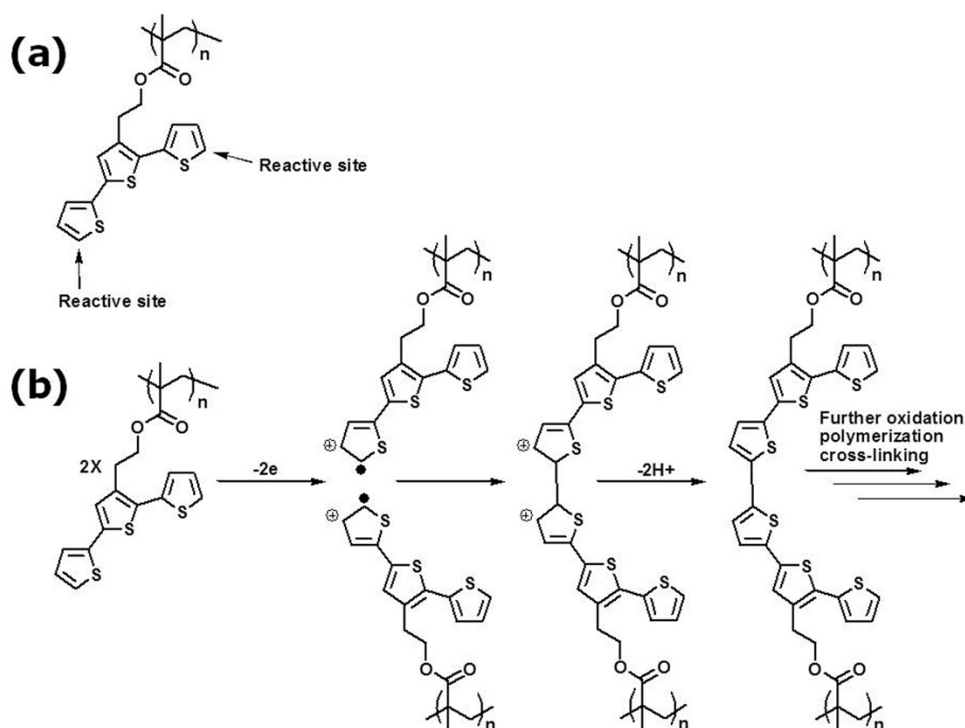


Figure 4. (a) Structure and reactive sites of grafted 3T-methacrylate pendent attached to the electropolymerized 3T-CTA RAFT agent backbone. (b) Mechanism showing the electropolymerization of pendent terthiophene groups.

Herein, conducting atomic force microscopy (C-AFM) was performed to investigate the nanopatterning on the precursor 3T-methacrylate brush films and examine the effects on the patterns by varying the applied bias and writing speed. The setup and oxidation mechanism can be seen in Figures 1 and 5 respectively. In general, an electrical bias between the AFM probe and the substrate can induce redox reactions on the surface species in the contact region (Figure 1). Conductive tips made of a variety of materials, such as doped silicon, boron, diamond, tungsten, tungsten carbide, and platinum-coated silicon nitride, have been used, in which patterns were achieved due to the application of the voltage bias between the AFM tip and the polymer film resulting in the formation of crosslinked polythiophene species. This occurs because anodic oxidation generates radical cations through the electroactive sites contained on the thiophene moieties (Figure 4a), providing the mechanism for electropolymerization (Figure 4b) [13]. The water meniscus plays an important role in the reactions (Figure 1) as it forms a bridge between the tip and the film covered substrate [11]. If sufficient voltage bias is applied, a localized oxidation over an area determined by the tip-sample contact occurs [41]. It is important to mention that attempts were made to use a nitrogen chamber. However, no apparent electrochemical patterning was observed under these inert (or dry) conditions. Therefore, only ambient conditions were used for further studies.

The information obtained from the localized electropolymerization of polymer brush based on the oxidation of the electroactive terthiophene pendent molecules can be seen in Figure 5. The AFM topographic images are shown in Figure 5a and b, while the AFM line profile heights of the films, obtained by varying either the writing speed or the applied bias, are plotted in Figure 5c and d. As shown in Figure 5a, four individual lines are evident after applying a constant voltage bias of -10 V at different writing speeds of 0.4, 0.6, 0.8, and 1.0 $\mu\text{m/s}$ (from left to right) performed under ambient conditions. The relative heights of the line patterns were determined using AFM profilometry with the corresponding lines, and were found to be 2.9, 2.7, 2.5, and 2.1 nm (Figure 5c), corresponding to the writing speeds of 0.4, 0.6, 0.8 to 1.0 $\mu\text{m/s}$, respectively. These results suggest that under a constant voltage bias, the height of the line patterns decreased linearly with increasing writing speed. Consequently, the contact time between the conductive tip and the specific location of the precursor polymer film exhibited good control over the pattern height. In other words, with fixed applied bias and at lower writing speeds, higher nanopatterns can be expected. The previous investigation showed a similar relationship between the pattern height and tip contact time, in which either spin-coated poly(vinylcarbazole) or LBL fabricated films were used to form nanopatterns under a constant bias [12,14]. Additional polymer brush thicknesses (<25 nm) were attempted to determine whether electro-nanopatterning could work on thinner polymeric brush films. However, for the case of 3T-methacrylate with thinner polymer brushes, no patterns were evident. Therefore, only this polymer brush thickness was investigated. The dependence of the pattern height as a function of voltage bias is shown in Figure 5b. Interestingly, after applying a constant writing speed of 0.4 $\mu\text{m/s}$ at different voltage bias ranging from -10, -8, -6 to -4 V (from left to right), only three individual lines are evident from -10, -8, to -6 V bias (Figure 5b) with corresponding heights of 3.0, 2.17, and 2.0 nm, respectively. In the case of the -4 V area, no pattern was evident.

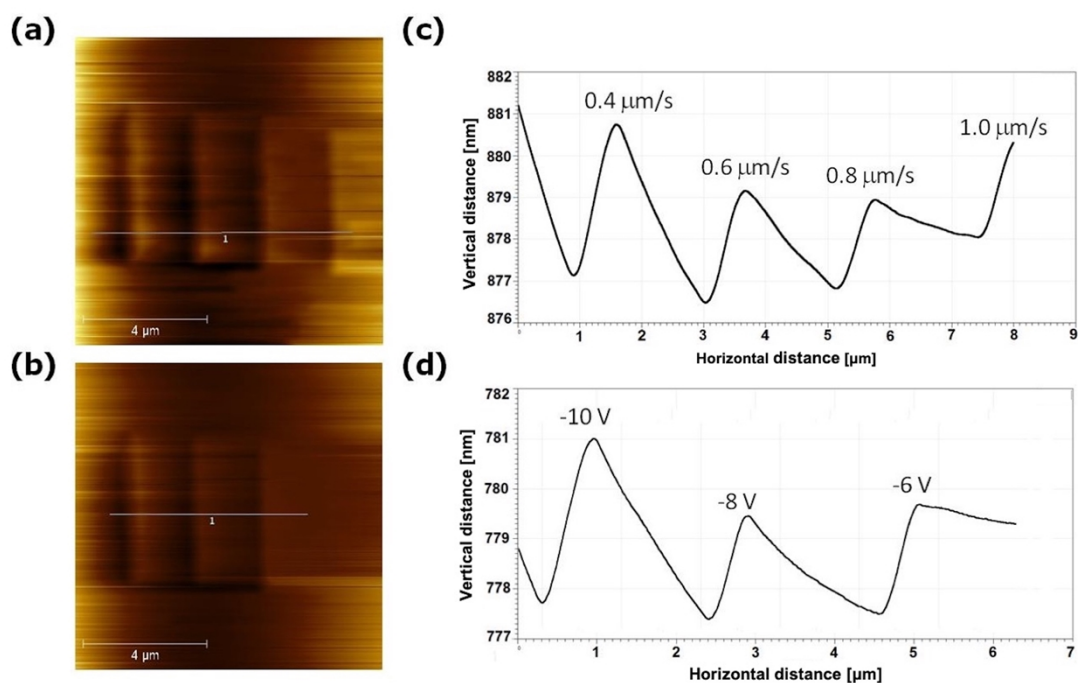


Figure 5. AFM topographic image (z range 10 nm) and line profiles of four lines pattern after (a, c) applying -10 V at different writing speeds of 0.4, 0.6, 0.8, and 1.0 $\mu\text{m/s}$ (from left to right) (b, d) a constant writing speed of 0.4 $\mu\text{m/s}$ at different voltage bias ranging from -10, -8, -6, to -4 V.

These observations suggest that the nanopattern generated by this method depends on the writing conditions (i.e. writing speed and applied voltage). However, it should be mentioned that the mechanism of forming these raised nanopatterns is not thoroughly understood even though similar observations have been reported for poly(methyl methacrylate) films. One theory is that the applied voltage increases the current through the polymer underneath the conducting AFM tip [13–16,19], which in turn increases the joule heating of the polymer film. When the polymer film is heated and cross-linking of the polymer chains occurs through electropolymerization, it is possible that the thermal expansion of the cross-linked materials gives rise to the raised nanostructures [14]. Although the AFM topography image determined using CS-AFM (contact mode) had less resolution than images obtained using tapping mode, clearer images were still obtained from the current images (Figure 6a and b). In these cases, the patterns were better seen due to color scale (or gray intensity) distribution [42]. The higher contrast was due to the difference in conductivity of the two materials with a high conductance corresponding to the crosslinked patterned regions [32].

In addition to giving better resolution images, the raised line results in the formation of electrically conducting nanopatterns due to the formation of extended π -conjugation of the terthiophene electroactive units via the electrochemical crosslinking to form polythiophene [19]. The increased conductivity was confirmed through the current map images (Figure 6a and b). For example, upon creating the patterns at different writing speeds (Figure 5a) of 0.4, 0.6, 0.8, and 1.0 $\mu\text{m/s}$ or voltage bias (Figure 6b) of -10, -8, -6, and -4 V, the images were then processed by scanning the patterned areas with an applied -3 V tip bias voltage at a rate of 1.5 lines/s. As seen in both cases, lower color contrasts in areas where the lines were produced were evident. These areas imply the relative differences in

conductivity. For example, Figure 6c shows the cross-sectional area of the patterned lines produced at the different writing speeds of 0.4, 0.6, 0.8, and 1.0 $\mu\text{m/s}$ (left to right) at a constant -10 V bias. From the graphical representation, the overall peak intensities (current) of the patterned areas were 0.8, 0.6, 0.5, and 0.4 pA, corresponding to the line created at writing speeds of 0.4, 0.6, 0.8, and 1.0 $\mu\text{m/s}$, respectively. Similarly, the cross-sectional area of the patterned lines produced at different voltages at -10, -8, -6, and -4 V, were examined (Figure 6d), and the relative intensities corresponding to these lines were 0.8, 0.7, 0.4, and ~ 0.0 pA, respectively. These lower current values in the created patterns are perhaps due to the application of the negative dc bias voltage.

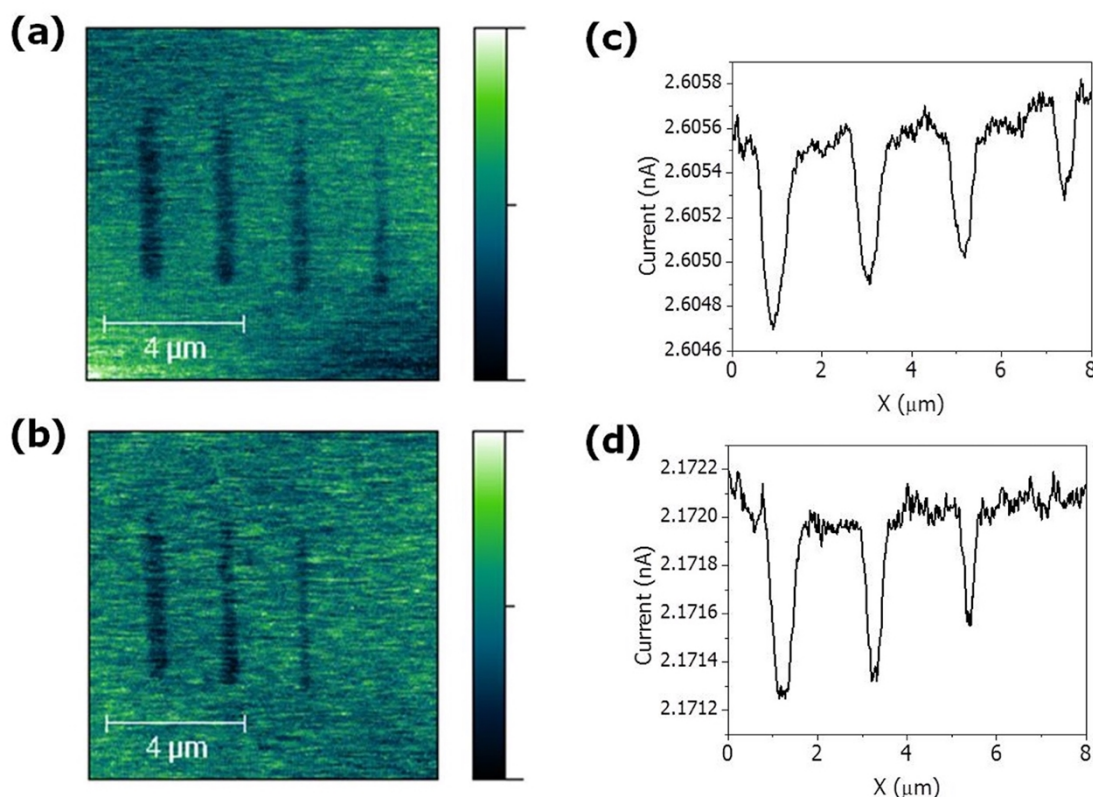


Figure 6. AFM current maps and current profiles of four lines patterned after (a, c) applying -10 V at different writing speeds of 0.4, 0.6, 0.8, and 1.0 $\mu\text{m/s}$ (from left to right) (b, d) a constant writing speed of 0.4 $\mu\text{m/s}$ at different voltage bias ranging from -10, -8, -6 to -4 V. (note topography images in Figure 5).

CS-AFM has been used to probe site specific conductivity and current-voltage (I-V) properties of polyaniline (PANI) films by using current flow through an Au-coated tip/PANI/ITO substrate [43–45]. Similarly, Tseng and co-workers have shown reversible conductivity changes of a PANI composite film (nanofiber/Au nanoparticle) using conductive AFM [44] and emphasized the possible application of nanoscale memory devices. Yang and co-workers also studied the conductivities of the pattern domains and their corresponding I-V responses in order to better understand the mechanism of nano-charging in poly(3,4-ethylenedioxythiophene) [46]. Herein, similar results with the current polymeric film should reveal similar characteristics.

To test this method, a single line on the polymer brush film using a writing speed of $0.4 \mu\text{m/s}$ and an applied bias of -10 V was performed. As seen from the AFM topography (Figure 7a) and current (Figure 7b) images, a distinct pattern was achieved. After formation of the pattern, we obtained two I-V curves (Figure 7c) using two distinct areas on the current map image (Figure 7b), i.e. crosslinked patterned (AFM tip positioned at arrow 1) and uncrosslinked brush (AFM tip positioned at arrow 2) areas. From the I-V curves, several different characteristics were displayed. In the case of arrow 1, this exhibited a typical junction, I-V curve of a conducting polymer, indicating that the conductivity in the local region increased after nanowriting. This conductivity increase may be attributed to the thinner resistor where an effect of both partial loss of the polymer brush and polymerization of terthiophene groups could be accounted. This observation also presents good proof that the formation of a conjugated polythiophene patterned area contains many energy states within the band gap [12,27,47]. Compared with the current image, the I-V curves gave a more quantitative sense with respect to the conductivity change, although the conductivity values cannot be directly calculated from this non-ohmic behavior. In contrast, the unpatterned brush area (AFM tip positioned at arrow 2) was depicted by a flat line in the I-V curve. This result is expected since this area is composed of the unconjugated, uncrosslinked brush. Finally, more complex patterns were drawn in order to demonstrate the facile patterning on these types of electroactive polymer brush surfaces. Figure 8 shows the 2-D topographic (Figure 8a and d), friction (Figure 8b and e), and current (Figure 8c and f) images of a series of boxes (Figure 8a-c) and the state of Texas map (Figure 8d-f) written at -10 V with a writing speed of $0.4 \mu\text{m/s}$. The average height of the pattern was determined to be 2.9 nm , which is somewhat consistent with the data presented earlier, using the same patterning conditions. Similarly, higher resolution friction images were also obtained (Figure 8b and e) to further confirm the successful formation of the two different patterns. Finally, the current images were also obtained again by sweeping at -3 V after patterning. It is clearly seen that the blue-green color contour showed a higher current flow through the boxes (Figure 8c) and the state of Texas (Figure 8f) patterns. In another words, the conductivity of the patterned areas was higher than the unpatterned domains as mentioned earlier.

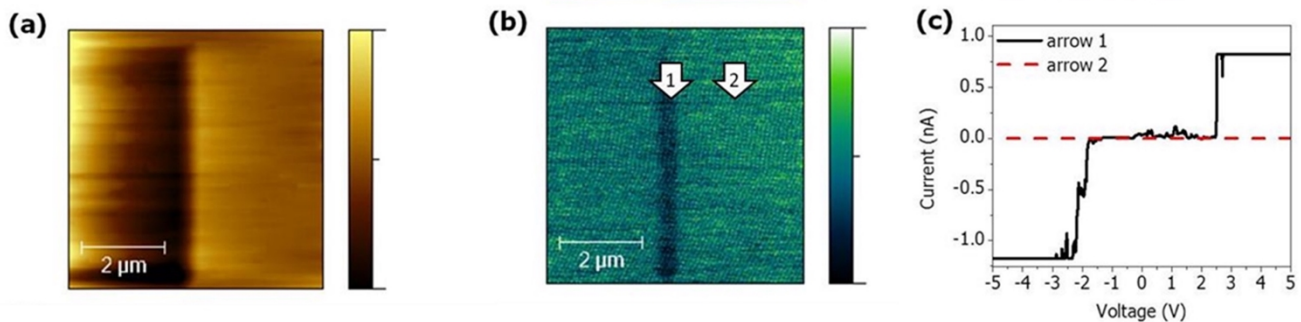


Figure 7. AFM (a) topography (z range 10 nm), and (b) current map of a single line created on electroactive film at -10 V at writing speed of $0.4 \mu\text{m/s}$. (c) I-V curves of different locations on the electroactive material.

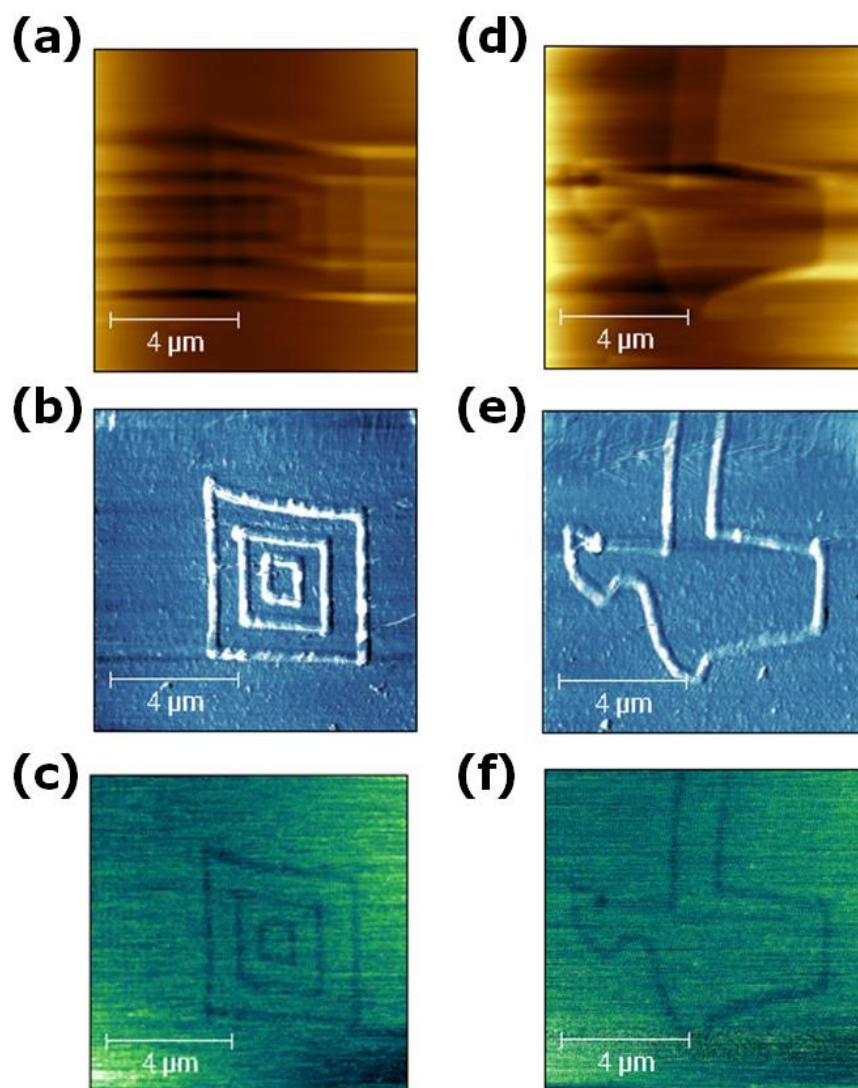


Figure 8. AFM images of (a-c) three squares and (d-f) the state of Texas, where the images correspond to the AFM (a and d) topography (z range 10 nm), (b and e) friction, and (c and f) current images.

4. Conclusion

The fabrication of pendant terthiophene polymer brushes as ultrathin films has been demonstrated using the SIP approach. UV-vis, ellipsometry, and AFM studies showed differences in the film structure at various stages of film development. These films were subsequently employed for the investigation of electrochemical nanopatterning using current sensing AFM as a writing technique. The dependence of the nanofeature properties on applied voltage and writing speed was studied. The pattern formation was demonstrated in order to show the possibility for future applications such as information storage devices and nanowires.

Acknowledgements

We acknowledge funding from the National Science Foundation (NSF): NSF-1608457 and NSF-1333651. The authors also acknowledge technical support from Park AFM Instruments, Thales Nano Inc. and Malvern-Panalytical Instruments Ltd. Work (or part of this work) was conducted by RC Advincula with the ORNL's Center for Nanophase Materials Sciences, which is a US Department of Energy Office of Science User Facility.

Conflict of Interests

The authors declare no conflict of interests.

References

- [1] M. Lutwyche, M. Despont, U. Drechsler, U. Dürig, W. Häberle, H. Rothuizen, R. Stutz, R. Widmer, G. Binnig, P. Vettiger, Highly parallel data storage system based on scanning probe arrays, *Appl. Phys. Lett.* 77 (2000) 3299–3301.
- [2] J. Lawrence, P. Andrew, W.L. Barnes, M. Buck, G. Turnbull, I. Samuel, Optical properties of a light-emitting polymer directly patterned by soft lithography, *Appl. Phys. Lett.* 81 (2002) 1955–1957.
- [3] Y. Huang, X. Duan, Q. Wei, C.M. Lieber, Directed assembly of one-dimensional nanostructures into functional networks, *Science*. 291 (2001) 630–633.
- [4] G. Liu, S.H. Petrosko, Z. Zheng, C.A. Mirkin, Evolution of Dip-Pen Nanolithography (DPN): From Molecular Patterning to Materials Discovery, *Chem. Rev.* 120 (2020) 6009–6047.
- [5] G. Liu, M. Hirtz, H. Fuchs, Z. Zheng, Development of Dip-Pen Nanolithography (DPN) and its derivatives, *Small*. 15 (2019) 1900564.
- [6] A. Pimpin, W. Srituravanich, Review on micro-and nanolithography techniques and their applications, *Eng. J.* 16 (2012) 37–56.
- [7] F.D.C. Siacor, Q. Chen, J.Y. Zhao, L. Han, A.D. Valino, E.B. Taboada, E.B. Caldoni, R.C. Advincula, On the Additive Manufacturing (3D Printing) of Viscoelastic Materials and Flow Behavior: From Composites to Food Manufacturing, *Addit. Manuf.* 45 (2021) 102043.
- [8] R.F. Pease, S.Y. Chou, Lithography and other patterning techniques for future electronics, *Proc. IEEE*. 96 (2008) 248–270.
- [9] W. Shim, A.B. Braunschweig, X. Liao, J. Chai, J.K. Lim, G. Zheng, C.A. Mirkin, Hard-tip, soft-spring lithography, *Nature*. 469 (2011) 516–520.
- [10] Y. Li, B.W. Maynor, J. Liu, Electrochemical AFM “dip-pen” nanolithography, *J. Am. Chem. Soc.* 123 (2001) 2105–2106.
- [11] L.G. Rosa, J. Liang, Atomic force microscope nanolithography: dip-pen, nanoshaving, nanografting, tapping mode, electrochemical and thermal nanolithography, *J. Phys. Condens. Matter*. 21 (2009) 483001.
- [12] C. Huang, G. Jiang, R. Advincula, Electrochemical Cross-Linking and Patterning of Nanostructured Polyelectrolyte–Carbazole Precursor Ultrathin Films, *Macromolecules*. 41 (2008) 4661–4670.
- [13] S. Jegadesan, R.C. Advincula, S. Valiyaveetil, Nanolithographic electropolymerization of a precursor polymer film to form conducting nanopatterns, *Adv. Mater.* 17 (2005) 1282–1285.

- [14] S. Jegadesan, S. Sindhu, R.C. Advincula, S. Valiyaveetil, Direct electrochemical nanopatterning of polycarbazole monomer and precursor polymer films: ambient formation of thermally stable conducting nanopatterns, *Langmuir*. 22 (2006) 780–786.
- [15] J.Y. Park, R. Ponnampati, P. Taraneekar, R.C. Advincula, Carbazole Peripheral Poly (benzyl ether) Dendrimers at the Air– Water Interface: Electrochemical Cross-Linking and Electronanopatterning, *Langmuir*. 26 (2010) 6167–6176.
- [16] J.Y. Park, P. Taraneekar, R. Advincula, Polythiophene precursor electrochemical nanolithography: highly local thermal and morphological characterization, *Soft Matter*. 7 (2011) 1849–1855.
- [17] E.B. Caldona, D.W. Smith Jr, D.O. Wipf, Surface electroanalytical approaches to organic polymeric coatings, *Polym. Int.* 70 (2021) 927–937.
- [18] A.C.C. de Leon, Í.G. da Silva, K.D. Pangilinan, Q. Chen, E.B. Caldona, R.C. Advincula, High performance polymers for oil and gas applications, *React. Funct. Polym.* 162 (2021) 104878.
- [19] R. Barbey, L. Lavanant, D. Paripovic, N. Schuwer, C. Sugnaux, S. Tugulu, H.-A. Klok, Polymer brushes via surface-initiated controlled radical polymerization: synthesis, characterization, properties, and applications, *Chem. Rev.* 109 (2009) 5437–5527.
- [20] S. Saha, G.L. Baker, Surface-tethered conjugated polymers created via the grafting-from approach, *J. Appl. Polym. Sci.* 132 (2015).
- [21] K. Wolski, A. Gruszkiewicz, M. Wytrwal-Sarna, A. Bernasik, S. Zapotoczny, The grafting density and thickness of polythiophene-based brushes determine the orientation, conjugation length and stability of the grafted chains, *Polym. Chem.* 8 (2017) 6250–6262.
- [22] M. Flejszar, P. Chmielarz, K. Wolski, G. Grześ, S. Zapotoczny, Polymer brushes via surface-initiated electrochemically mediated ATRP: role of a sacrificial initiator in polymerization of acrylates on silicon substrates, *Materials*. 13 (2020) 3559.
- [23] J.O. Zoppe, N.C. Ataman, P. Mocny, J. Wang, J. Moraes, H.-A. Klok, Surface-initiated controlled radical polymerization: state-of-the-art, opportunities, and challenges in surface and interface engineering with polymer brushes, *Chem. Rev.* 117 (2017) 1105–1318.
- [24] Y. Stetsyshyn, J. Raczowska, K. Harhay, K. Gajos, Y. Melnyk, P. Dąbczyński, T. Shevtsova, A. Budkowski, Temperature-responsive and multi-responsive grafted polymer brushes with transitions based on critical solution temperature: Synthesis, properties, and applications, *Colloid Polym. Sci.* 299 (2021) 363–383.
- [25] A. Bunha, P.-F. Cao, J.D. Mangadlao, R.C. Advincula, Cyclic poly (vinylcarbazole) via ring-expansion polymerization-RAFT (REP-RAFT), *React. Funct. Polym.* 80 (2014) 33–39.
- [26] S. Perrier, P. Takolpuckdee, C.A. Mars, Reversible addition– fragmentation chain transfer polymerization: end group modification for functionalized polymers and chain transfer agent recovery, *Macromolecules*. 38 (2005) 2033–2036.
- [27] C.D. Grande, M.C. Tria, G. Jiang, R. Ponnampati, R. Advincula, Surface-grafted polymers from electropolymerized polythiophene RAFT agent, *Macromolecules*. 44 (2011) 966–975.
- [28] C.L. Gaupp, J.R. Reynolds, Multichromic copolymers based on 3, 6-bis (2-(3, 4-ethylenedioxythiophene))-N-alkylcarbazole derivatives, *Macromolecules*. 36 (2003) 6305–6315.
- [29] Z. Chen, E. Villani, S. Inagi, Recent progress in electropolymerization methods toward one-dimensional conducting polymer structures, *Curr. Opin. Electrochem.* 28 (2021) 100702.
- [30] I.F. Perepichka, D.F. Perepichka, *Handbook of Thiophene-Based Materials: Applications in Organic Electronics and Photonics*, 2 Volume Set, John Wiley & Sons, 2009.

- [31] A.C. de Leon, R.E.S. Imperial, Q. Chen, R.C. Advincula, One-Step Fabrication of Superhydrophobic/Superoleophilic Electrodeposited Polythiophene for Oil and Water Separation, *Macromol. Mater. Eng.* 304 (2019) 1800722.
- [32] A.C.C. de Leon, R.B. Pernites, R.C. Advincula, Superhydrophobic colloiddally textured polythiophene film as superior anticorrosion coating, *ACS Appl. Mater. Interfaces.* 4 (2012) 3169–3176.
- [33] U. Evans-Kennedy, J. Clohessy, V.J. Cunnane, Spectroelectrochemical Study of 2, 2'-5', 2''-Terthiophene Polymerization at a Liquid/Liquid Interface Controlled by Potential-Determining Ions, *Macromolecules.* 37 (2004) 3630–3634.
- [34] A. Yassar, C. Moustrou, H.K. Youssoufi, A. Samat, R. Guglielmetti, F. Garnier, Synthesis and characterization of poly (thiophenes) functionalized by photochromic spironaphthoxazine groups, *Macromolecules.* 28 (1995) 4548–4553.
- [35] J.D. Mangadlao, A.C.C. De Leon, M.J.L. Felipe, P. Cao, P.A. Advincula, R.C. Advincula, Grafted carbazole-assisted electrodeposition of graphene oxide, *ACS Appl. Mater. Interfaces.* 7 (2015) 10266–10274.
- [36] G.A. Sotzing, J.R. Reynolds, P.J. Steel, Electrochromic conducting polymers via electrochemical polymerization of bis (2-(3, 4-ethylenedioxy) thienyl) monomers, *Chem. Mater.* 8 (1996) 882–889.
- [37] U. Geissler, M. Hallensleben, N. Rohde, Electrically conductive copolymers based on 1-methylpyrrole, *Synth. Met.* 84 (1997) 173–174.
- [38] R. Schrebler, P. Grez, P. Cury, C. Veas, M. Merino, H. Gomez, R. Cordova, M. Del Valle, Nucleation and growth mechanisms of poly (thiophene) Part 1. Effect of electrolyte and monomer concentration in dichloromethane, *J. Electroanal. Chem.* 430 (1997) 77–90.
- [39] P. Taranekar, T. Fulghum, A. Baba, D. Patton, R. Advincula, Quantitative electrochemical and electrochromic behavior of terthiophene and carbazole containing conjugated polymer network film precursors: EC-QCM and EC-SPR, *Langmuir.* 23 (2007) 908–917.
- [40] K. Kaneto, K. Yoshino, Y. Inuishi, Electrical and optical properties of polythiophene prepared by electrochemical polymerization, *Solid State Commun.* 46 (1983) 389–391.
- [41] J. Song, M.A. Hempenius, H.J. Chung, G.J. Vancso, Writing nanopatterns with electrochemical oxidation on redox responsive organometallic multilayers by AFM, *Nanoscale.* 7 (2015) 9970–9974.
- [42] R.B. Pernites, E.L. Foster, M.J.L. Felipe, M. Robinson, R.C. Advincula, Patterned surfaces combining polymer brushes and conducting polymer via colloidal template electropolymerization, *Adv. Mater.* 23 (2011) 1287–1292.
- [43] C.-G. Wu, S.-S. Chang, Nanoscale Measurements of Conducting Domains and Current– Voltage Characteristics of Chemically Deposited Polyaniline Films, *J. Phys. Chem. B.* 109 (2005) 825–832.
- [44] R.J. Tseng, J. Huang, J. Ouyang, R.B. Kaner, Y. Yang, Polyaniline nanofiber/gold nanoparticle nonvolatile memory, *Nano Lett.* 5 (2005) 1077–1080.
- [45] E.B. Caldona, A.C.C. de Leon, B.B. Pajarito, R.C. Advincula, Novel anti-corrosion coatings from rubber-modified polybenzoxazine-based polyaniline composites, *Appl. Surf. Sci.* 422 (2017) 162–171.
- [46] J. Ouyang, C. Chu, F. Chen, Q. Xu, Y. Yang, High-conductivity poly (3, 4-ethylenedioxythiophene): poly (styrene sulfonate) film and its application in polymer optoelectronic devices, *Adv. Funct. Mater.* 15 (2005) 203–208.
- [47] H.J. Lee, S.-M. Park, Electrochemistry of conductive polymers. 30. Nanoscale measurements of doping distributions and current– voltage characteristics of electrochemically deposited Polypyrrole films, *J. Phys. Chem. B.* 108 (2004) 1590–1595.